ACS Photonics

Article

pubs.acs.org/journal/apchd5

Plasmon-Modulated Photoluminescence of Single Gold Nanobeams

Albert Wan,[†,#] Tao Wang,[†,#] Tingting Yin,[‡] Anran Li,[§] Hailong Hu,[‡] Shuzhou Li,[§] Ze Xiang Shen,[‡] and Christian A. Nijhuis[*,†,∥,⊥]

[†]Department of Chemistry, National University of Singapore, 3 Science Drive 3, Singapore 117543, Singapore

[‡]Centre for Disruptive Photonic Technologies, School of Physical and Mathematical Sciences, Nanyang Technological University, 21 Nanyang Link, Singapore 637371, Singapore

[§]School of Materials Science and Engineering, Nanyang Technological University, 50 Nanyang Avenue, Singapore 639798, Singapore

[∥]Solar Energy Research Institute of Singapore (SERIS), 7 Engineering Drive 1, National University of Singapore, Singapore 117574, Singapore

[⊥]Centre for Advanced 2D Materials and Graphene Research Centre, National University of Singapore, 2 Science Drive 6, Singapore 117546, Singapore

Supporting Information

ABSTRACT: In this work, we investigate the modulation of the photoluminescence (PL) of a single Au nanobeam (NB) by the surface plasmons of a Ag nanowire (NW) and the gap plasmons between the two nanostructures. By changing the polarization of the laser that excites the nanostructure and controlling the separation distance d between the two nanostructures, we found that the transverse surface plasmon resonance of the Ag NW enhanced the PL (at 520 nm) of the Au NB with a maximum effect at d = 7 nm. The PL enhancement (at 520 nm) was quenched and a new PL peak was observed at a longer wavelength for d < 7 nm. The PL quenching effect could be understood by the quadrupole-like plasmonic resonance between the Ag NW and the Au NB and be qualitatively explained by the mode dispersion as a function of d obtained using the transfer matrix transmittance calculation. FDTD simulations show that the new PL peak at a longer wavelength is caused by the waveguide-mode gap plasmons between the Au NB and the Ag NW.

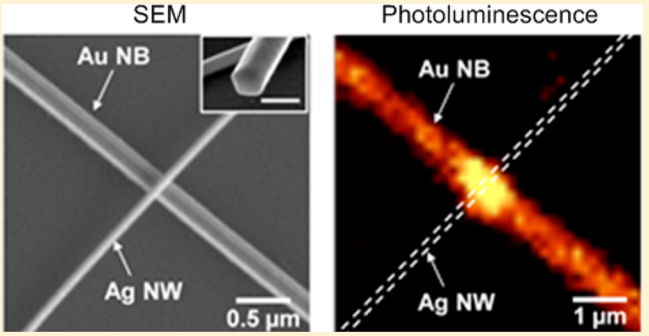

KEYWORDS: *gold photoluminescence, surface plasmon, gap plasmon, gold nanobeam nanoskiving, silver nanowires, photoluminescence enhancement*

Photoluminescence (PL) of gold nanostructures has attracted attention in recent years because of its potential applications in bioimaging,[1−4] sensing,[5,6] and plasmonic mode mapping.[7−9] The origin of the PL of bulk gold has been understood as the radiative recombination of interband transitions of d-band electrons or intraband transitions of electrons within the d-band.[10,11] Unlike fluorophores that have inevitable limitations of photobleaching and photoblinking, PL of gold nanostructures is thermally robust.[1−9] Moreover, gold nanostructures are biocompatible for biological applications such as cell imaging and biosensing.[1−6] However, the low PL efficiencies of gold nanostructures (the measured quantum yield reported to be $\sim 10^{-6}$–10^{-5}) may limit their usefulness.[1,3,12−14] Therefore, understanding the mechanisms of enhancing the PL efficiency of gold nanostructures is important.

One way to improve the PL efficiency of gold nanostructures is to utilize surface plasmon resonances. Recent studies have revealed that the PL of isolated gold nanostructures can be modulated and enhanced by their own localized surface plasmon resonances owing to the coupling between excited electron−hole pairs and the collective oscillating free electrons.[12−17] PL of gold can also be enhanced by plasmonic resonators made of different types of nanomaterials such as Ag nanowires,[18] Au nanospheres,[19] and Au nanodisk arrays.[20] Since gold itself is a plasmonic material, it is straightforward to form plasmonic interactions such as gap plasmons between gold and other plasmonic resonators. To avoid the possible *quenching*, however, the plasmonic resonators should not be too close to the gold nanostructures. It is well known that when luminophores are too close (e.g., < 10 nm) to plasmonic resonators, PL of the luminophores may be reduced via nonradiative energy transfer from the excited luminophores to the plasmonic resonators.[21] Therefore, to optimize the PL efficiency, it is important to study the distance dependence of the plasmon-enhanced PL of a gold nanostructure. Moreover, the localized surface plasmon resonance of metal nanostructures may alter the spectral profiles of the luminophores around

Received: June 21, 2015
Published: August 20, 2015

DOI: 10.1021/acsphotonics.5b00341
ACS Photonics 2015, 2, 1348−1354

the nanostructures.[22−24] In this case, by changing the separation distance d between a gold nanostructure and the plasmonic nanostructures, not only the intensity of the PL but also the peak position and spectral shape of the PL are expected to be modulated by the localized surface plasmons.

In this work, we investigated the plasmonic effect of a chemically synthesized Ag nanowire (NW)[25] on the PL of a Au nanobeam (NB)[26] fabricated by nanoskiving,[27] which involves sectioning of chemically grown crystalline Au microplates. We found that by bringing the Ag NW closer to the Au NB through decreasing the thickness of the dielectric spacer between the two nanostructures, the PL (peaked at 520 nm) of the Au NB was enhanced by locally enhanced electric fields resulting from the plasmonic interaction between the transverse plasmonic mode of the Ag NW and the Au NB with a maximum enhancement of 1.92 for d = 7 nm. In contrast, if the Ag NW was too close (d < 7 nm) to the Au NB, *quenching* of the PL enhancement and the appearance of a new emission peak at longer wavelengths (with the maximum changing from 610 nm to 685 nm with decreasing d from 7 nm to 3 nm) in the PL spectra were observed. The *quenching* of PL enhancement may be due to the quadrupole-like plasmonic resonance between the Ag NW and the Au NB, which causes reduced far-field scattering.[28−30] A qualitative understanding of the quenching effect was obtained by using transfer matrix transmittance calculation. Our FDTD (finite-difference time-domain) simulations show that the new PL peaks at longer wavelengths result from the modulation of the PL by the well-defined waveguide-mode gap plasmons[18,31] between the Au NB and the Ag NW.

RESULTS AND DISCUSSION

To study the enhancement and modulation of the PL of a single Au nanobeam via plasmonic effects, we prepared cross-like structures of a Au NB and a Ag nanowire, as shown schematically in Figure 1. Unlike in experiments involving continuous metal gold films, the confined gold nanostructures provide us the possibility to image the location of PL enhancement on the Au NB and to confirm the enhancement occurring at the intersection of the two nanostructures. The single crystalline Au NBs were fabricated using a method called "nanoskiving", which involves sectioning chemically synthesized Au microplates embedded in epoxy (see Methods) using a ultramicrotome (a standard tool to cut samples into thin slices for, for example, analysis by transmission electron microscope) for two reasons.[25,26,32,33] First, the Au NBs are single crystalline, which reduces the plasmonic damping. Second, the Au NBs are stabilized by surrounding epoxy, which makes it possible to handle individual Au NBs, facilitating the fabrication process and the yield in cross-like structures considerably.

The details of the sample preparation are indicated as follows. The Ag NWs were synthesized by using the polyol method,[25] and the Au microplates were synthesized by reducing $HAuCl_4$ in ethylene glycol in the presence of polyvinylpyrrolidone (PVP).[26] We drop-casted the suspensions of Au microplates on a flat piece of epoxy slab (Figure 1a). After drying, we rinsed the microplates on the slab with ethanol and ultrapure water (18.2 MΩ·cm) and then embedded the slab in additional epoxy (Figure 1b). We sectioned the microplates surrounded by epoxy using an ultramicrotome equipped with a diamond knife to form Au NBs (Figure 1c). We transferred the resulting epoxy thin films (50 nm thick) containing Au NBs onto a Si wafer, which had 300 nm thick SiO_2 on the surface, and removed the epoxy using an air-plasma

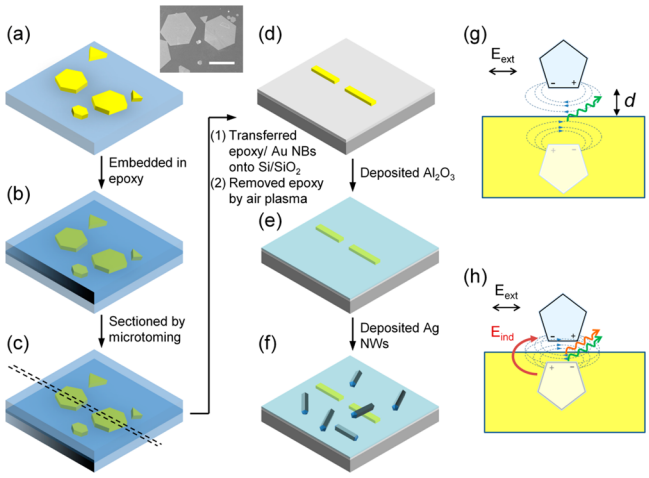

Figure 1. Schematic diagrams and the sample preparation procedure. (a) Chemically synthesized Au microplates were deposited on a thin (a few hundred micrometers) slab of epoxy. The inset shows the SEM image of the microplates. Scale bar: 50 μm. (b) The slab with the microplates was embedded in epoxy. (c) The microplates with surrounded by epoxy were sectioned by an ultramicrotome to form the Au NBs. (d) The epoxy films with Au NBs were transferred onto a piece of Si/SiO_2 wafer, followed by treatment with air-plasma to remove the epoxy. (e) A layer of Al_2O_3 with a thickness of 3−15 nm was deposited on the Au NBs and the substrate. (f) Chemically synthesized Ag NWs in ethanol were drop-casted on the substrate and were blown to dryness in a stream of N_2. The combined structure of a Ag NW aligned (almost) perpendicularly on top of a Au NB with the dielectric spacer could be found and was used for the PL measurements. (g and h) Cross-sectional diagrams of the Ag NW and the Au NB when d is relative large and small, respectively. The dashed lines indicate the direction of the electric field. The PL of Au is modulated by the electromagnetic interaction between the two nanostructures. The dense dashed lines in (h) indicate a stronger plasmonic interaction for a smaller gap than for the larger gap depicted in (g). The green arrows in (g) and (h) indicate the enhanced PL by the locally enhanced field due to the quadrupole-like plasmonic resonance between the Ag NW and the Au NB. The orange arrow in (h) indicates the waveguide-mode gap plasmon resonance at longer wavelengths. The E_z field distribution of the quadrupole-like plasmonic resonance and the gap plasmon resonance are shown in the Supporting Information Figure S1.

cleaner (Figure 1d). We deposited 3−15 nm thick Al_2O_3 on the substrate by using atomic layer deposition (ALD) as the dielectric spacer (Figure 1e) and then drop-casted the suspensions of Ag NWs on the substrate (Figure 1f). After drying under a stream of N_2, the Ag NWs were randomly distributed on the substrate. We selected the Ag NW that was (nearly) perpendicularly aligned on top of the Au NB using an optical microscope for the PL measurements (Figure 1f and see later Figure 3 for experimental data).

We controlled the thickness of Al_2O_3, changed the polarization angles of the excitation laser to modulate the plasmon modes between the Au NB and the Ag NW, and measured the corresponding PL spectrum of the Au NB to determine how surface plasmons of the Ag NW affect the PL of the Au NB. When d between the Ag NW and the Au NB is within a few tens of nanometers, the PL from Au is expected to be enhanced because of the locally enhanced field due to the plasmonic interaction between the Ag NW and the Au NB (Figure 1g). When d is small enough, the dipole-like surface plasmon resonance of the Ag NW can strongly couple to its

DOI: 10.1021/acsphotonics.5b00341
ACS Photonics 2015, 2, 1348−1354

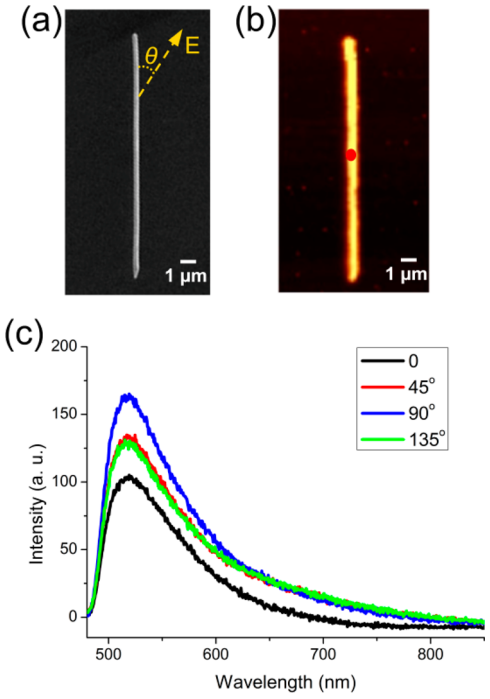

Figure 2. Photoluminescence of a single Au nanobeam. (a) SEM and (b) PL images of a single Au NB (width ~210 nm). (c) Corresponding PL spectra collected from the Au NB under a 457 nm laser excitation at different polarization angles. The polarization angles (θ) of 0° and 90° indicate that the excitation laser was polarized parallel and perpendicular to the long axis of the NB, respectively. The red dot in (b) indicates the region where the PL signals were collected.

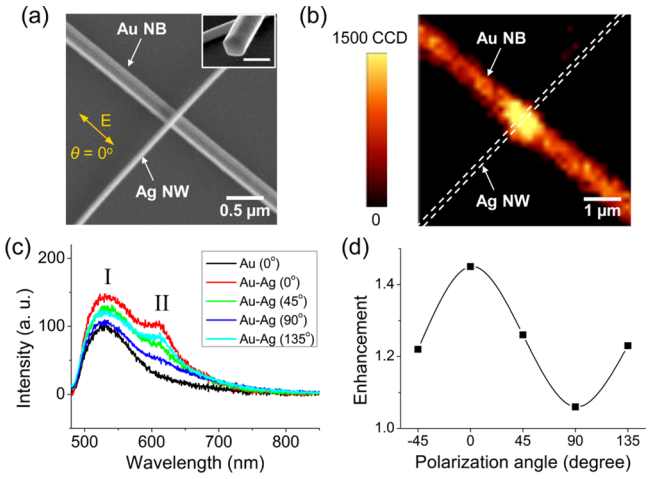

Figure 3. Photoluminescence of the Au NB-Ag NW cross-like nanostructure. (a) SEM image of a Ag NW aligned nearly perpendicular on a single Au NB (width ~150 nm) coated with 6 nm of Al_2O_3. The inset shows the SEM image of the cross-section of a Ag NW. Scale bar: 100 nm. (b) PL image of the nanostructure shown in (a). The sample was excited by a 457 nm laser with polarization angle perpendicular (θ = 0°) to the long axis of the Ag NW. (c) PL spectra collected at the Au NB and at the intersection of the nanostructures with different laser polarization angle θ. (d) Enhancement of PL intensities at 520 nm versus the polarization angles of the excitation laser.

image dipole on the Au surface to form either a quadrupole-like plasmonic resonance[28−30] or a waveguide-mode-like gap plasmon resonance,[18,31] which is expected to modulate the PL of Au (Figure 1h).

Before conducting the PL measurement for the combined structure of a Ag NW aligned on a Au NB, we first investigated the PL characteristics of a single Au NB using a confocal microscope. During the PL measurement, the NB was excited by a linearly polarized laser (λ_{exc} = 457 nm) at a normal incidence angle through an objective above the sample, and PL spectrum was recorded through the same objective as a function of the polarization angle (θ) of the aser excitation (see Methods). We acquired SEM images of the same Au NBs after the PL measurements so we could relate the optical properties to the structures in detail.

Figure 2a shows a SEM image of a typical Au NB that had a width of 210 nm, a length of 15.5 μm, and a thickness of ~50 nm. Figure 2b and c show the PL image collected under laser polarization perpendicular to the long axis of the Au NB (θ = 90°) and the PL spectra excited with θ ranging from 0° to 135°, respectively. The PL peak of the Au NB was observed to occur at ~520 nm (Figure 2c), which corresponds to the radiative recombination of electrons in the sp band at the Fermi level (near the L point in the first Brillion zone) of gold with holes in the d band below the Fermi level.[11,19] The maximum and minimum intensities of the PL were observed when the laser polarization was perpendicular (θ = 90°) and parallel (θ = 0°) to the long axis of the NB, respectively. This indicates that the PL was enhanced by the transverse surface plasmon resonance (TSPR) of the Au NB.

Figure 3a presents the PL measurement recorded on a cross-like structure with a Ag NW aligned (almost) perpendicularly with respect to a Au NB (width ~150 nm) coated with 6 nm of Al_2O_3. The inset of Figure 3a shows the SEM image of the pentagonal cross-section of the Ag NW. The PL image (Figure 3b) shows the enhancement of the PL at the intersection of the Ag NW and Au NB when the polarization of the excitation laser was perpendicular to the Ag NW (θ = 0°) to excite the TSPR mode of the Ag NW. Importantly, no PL signal from the Ag NW was observed. Moreover, it is important to mention that the absolute PL emission rate from the intersection area is higher than that from bulk gold (Supporting Information S2).

To determine the enhancement factor of the PL, PL spectra at the intersection of the two nanostructures and on the Au NB around 2 μm away from the intersection were measured (Figure 3c). We found that the enhancement of the PL intensity at 520 nm was dependent on the polarization angle of the excitation laser (Figure 3d) and reached a maximum (by a factor of 1.7) when the excitation laser was polarized perpendicularly to the long axis of the Ag NW. This observation indicates that the PL enhancement of the Au NB was due to the TSPR of the Ag NW. Figure 3c shows a new emission peak at ~620 nm in the PL spectra when the polarization of the excitation laser was not parallel to the long axis of the Ag NW (θ > 0°). Here we labeled the PL peak at 520 nm as peak I, and the new emission peak as peak II. On the basis of the results of FDTD simulations, we attribute the peak II to the PL modulation by the gap plasmon mode between the Ag NW and the Au NB (see below). It should be noted that the width of the Au NB used in Figure 3 (~150 nm) is smaller than that in Figure 2 (~210 nm), resulting in a reduction of the PL signal at peak I.

To confirm that peak II originates from the gap plasmon modes, we recorded the PL spectra as a function of d (Figure 4). The PL enhancement factor R (the ratio between the PL

DOI: 10.1021/acsphotonics.5b00341
ACS Photonics 2015, 2, 1348−1354

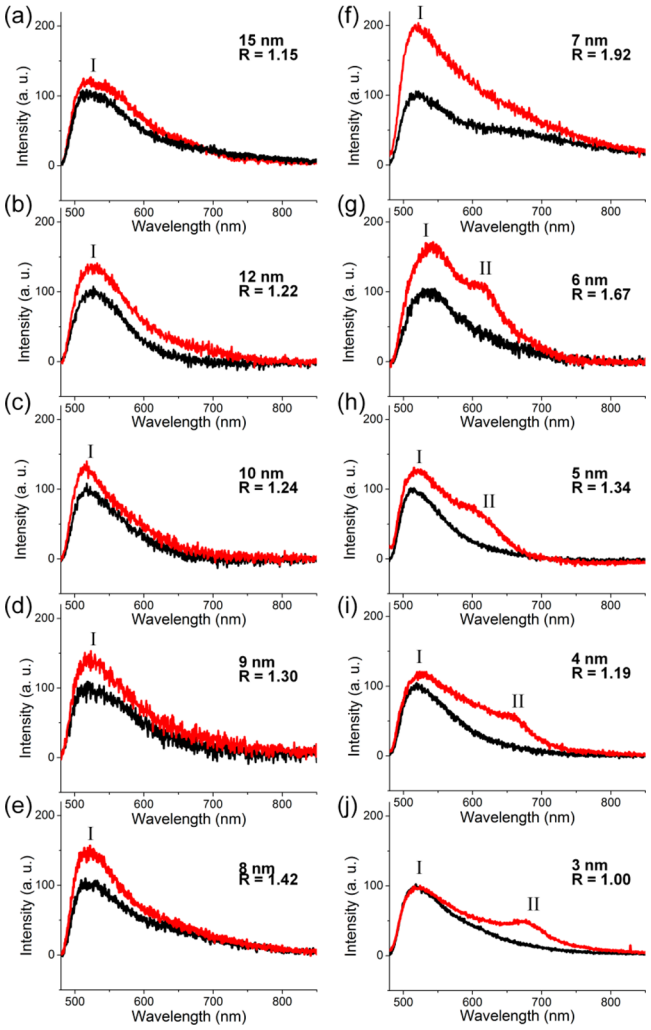

Figure 4. PL spectra of single Ag NWs (width ~70 nm) aligned perpendicularly on single Au NBs (width ~150 nm) with different thicknesses of Al_2O_3 between the nanostructures. The red and black curves are the PL spectra collected at the intersection and on the Au NB, respectively. The separation distance (d) between the Au NB and Ag NW and the PL enhancement factor (R) is indicated in the spectra. The excitation laser (λ = 457 nm) was polarized perpendicular (θ = 0°) to the long axis of the Ag NW during the measurement.

intensity at the Ag NW−Au NB intersection and that at the Au NB at peak I) and the PL spectral profile at the intersection of the Au NB and the Ag NW both depend on d. From the PL spectra shown in Figure 4 we make the following five observations. (i) R increases from 1.12 to 1.74 when d decreases from 15 to 7 nm and reaches its maximum value at d = 7 nm. The value of R decreases to 0.98 when d decreases from 7 nm to 3 nm (Figure 5a). (ii) A new emission peak (peak II) appears between 600 and 700 nm in the PL spectra for structures with d < 7 nm (Figure 4g−j). (iii) The position of peak II red shifts with decreasing d (Figure 5b). (iv) The PL enhancement of peak II increases with decreasing d (Figure 5b). (v) The PL enhancement factor of peak II (R_G) is larger than the PL enhancement factor R of peak I with d < 7 nm (Figure 5a,b).

The behavior of the PL enhancement at peak I (~520 nm) can be generally interpreted by the image-charge model,[18,28−30] where dipole oscillations of the TSPR of the Ag NW couple to its image dipoles of opposite charge distributions on the

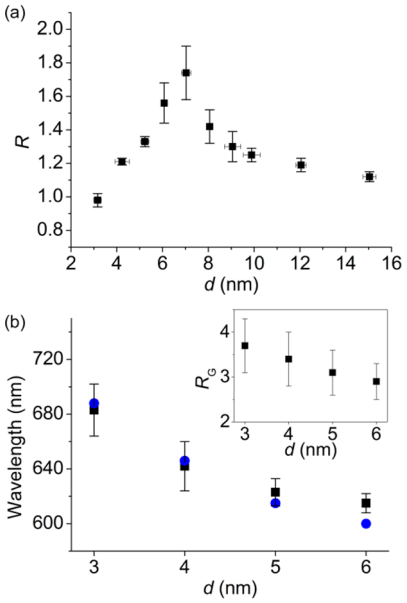

Figure 5. (a) PL enhancement factor of peak I (R) versus d. The error bars result from the standard deviation of three independent sample preparations and measurements. (b) Measured PL peak wavelengths (peak II, black dots) and simulated scattering peak wavelengths (blue dots) versus d. The inset shows the measured PL enhancement factor of peak II (R_G) with different gap sizes.

underlying Au surface (Figure 1h). When the separation d between the Ag NW and the Al_2O_3 layer decreases, the plasmonic resonance of the Ag NW enhances the local field between the Ag NW and the Au NB and thus increases the PL of the Au NB. On the other hand, as the Ag NW approaches the Au NB, the interaction between the dipole of the plasmonic resonance of the Ag NW and its image dipole in the Au NB becomes stronger and a quadrupole-like resonance forms between the two nanostructures.[28−30] The quadrupole-like resonance largely diminishes the far-field scattering of the structure and thus reduces the detected PL of the Au NB in the far field, which is similar to the case of Au or Ag nanoparticles on Au films.[29,30]

Theoretical calculations using the transfer matrix method provided a qualitative understanding of PL enhancement at peak I ≈ 520 nm (see Methods). Figure 6a shows how the mode dispersion changes as a function of wavelength and the separation d. The calculation results agree well with the experimental observations in Figure 5a. At 520 nm, the transmittance increases when d decreases to about 7 nm and decreases when d decreases from 7 nm to 3 nm. As the transmittance was calculated with $k = k_0\lambda/D \approx 7-10k_0$ (large spatial confinement), where D is the diameter of the Ag NW, the transmittance describes the near-field coupling of the fields in the intersection area and shows the ability of local field enhancement in the gap and the ability to transfer the local field enhancement out of the gap. Thus, this transmittance (at high k) describes both the local field enhancement for PL and the ability to transfer the PL to the far field and reflects the PL enhancement changes of peak I at 520 nm.

The FDTD simulations reveal that peak II correlates to the resonance of the gap plasmon modes. The FDTD-simulated scattering spectra (Figure 6b) show that a gap plasmon mode becomes more and more pronounced as d decreases. The electric field distribution (Figure 6c−f) shows that the field

DOI: 10.1021/acsphotonics.5b00341
ACS Photonics 2015, 2, 1348−1354

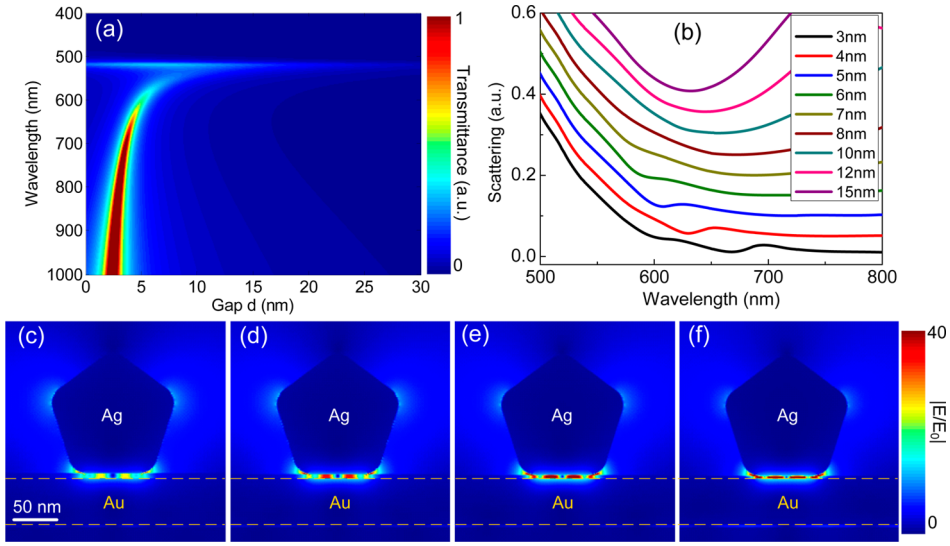

Figure 6. (a) Mode dispersion of the Ag NW−Au NB combined nanostructure with different gap size *d*. (b) FDTD-simulated scattering spectra of the Ag NW−Au NB combined nanostructure with different gap size *d*. FDTD-simulated electric field distributions of the Ag NW−Au NB cross-like nanostructures with different gap size for d = 6 at 600 nm (c), d = 5 at 615 nm (d), d = 4 at 646 nm (e), and d = 3 at 688 nm (f).

enhancement between the Au NB and the Ag NW resulted from this gap plasmon mode (field enhancement simulations at 457 and 520 nm are shown in Figures S3 and S4, respectively). The resonance wavelength of the gap plasmon mode red shifts and the local field in the gap becomes more intensive as *d* becomes smaller. This trend is also observed in the mode dispersion calculated with the transfer matrix method (Figure 6a). Meanwhile, the field distribution of the gap plasmon mode is very similar to the waveguide-mode gap plasmons between a Ag nanocube and a gold film.[31] We found that the measured PL peak (peak II) closely follows the calculated scattering peaks due to gap plasmons (Figure 5b). Thus, we attribute the new emission that appears when d = 3−6 nm to the PL of Au NB modulated by the gap plasmons. The PL was enhanced by the gap plasmon mode with R_G ranging from 2.9 to 3.7 when *d* decreased from 6 nm to 3 nm (inset of Figure 5b). Compared to the FDTD-simulated field enhancement, this gap-plasmon-modulated PL enhancement is much lower. One possible reason is that the PL is measured in the far field and the FDTD simulation shows the field enhancement in the near field. Thus, a far-field scattering factor should also be considered. Nevertheless, it clearly shows that PL enhancement increases as the field enhancement in the gap increases. Moreover, similar to our previous findings,[18] the PL peak II red shifts as the diameter of Ag NW increases (Supporting Information Section S3). Thus, to identify the gap effect of the enhanced PL, we used nearly constant Au NB widths (~150 nm) and Ag NW diameters (~70 nm).

We also notice that the measured PL enhancement of peak II (R_G) is larger than that of peak I (R). For example, with d = 3 nm, R_G is 3.7 (at 683 nm) and R is 0.98 (at 520 nm). This phenomenon can be understood by the following equation:[19,20]

$$R_{PL}(\omega_{em}) \propto \sigma_{scatt}(\omega_{em}) \left| \frac{E(\omega_{em})}{E_0(\omega_{em})} \right|^2 \quad (1)$$

where $R_{PL}(\omega_{em})$ is the emission enhancement of the gold PL. The term $R_{PL}(\omega_{em})$ is determined by the emission field enhancement and the far-field scattering coefficient $\sigma_{scatt}(\omega_{em})$ of the plasmonic structures. For the case d = 3 nm, $R_{PL}(\omega_{em})$ at both peak I (520 nm) and peak II (688 nm) can be calculated by the field enhancement and the far-field scattering coefficient from FDTD simulations. The field enhancement is about 8 and 40 times for 520 and 688 nm, respectively, while the scattering coefficient is about 0.25 and 0.035 for 520 and 688 nm, respectively (Figure 6 and Figure S4). Thus, the ratio of PL enhancement at peak I and peak II is about 3.5, which is close to the experimentally deduced ratio 3.78.

On the basis of the results of experimental measurements and theoretical simulations, we proposed the following mechanism. The interband transition of Au occurs to generate an electron−hole pair as the Au NB absorbs 457 nm photons from the excited laser. With the presence of a Ag NW on top of the Au NB with the separation distance between 7 and 15 nm, the localized electric fields generated by the TSPR of the Ag NW enhance the PL intensity of the Au NB. When the separation distance between the two nanostructures is smaller than 7 nm, the gap plasmons between the two nanostructures become significant. The gap plasmons modulate the PL of the Au NB and enhance the PL process at the resonance wavelength (600−700 nm). We cannot, however, exclude the possibility that peak II may be due to the radiative decay of the gap plasmons only or the combination of both emission (gap plasmons and PL) pathways in the last step.

CONCLUSIONS

This work shows that the PL of the Au NB can be enhanced by the TSPR of a Ag NW and modulated by the gap plasmons between the two nanostructures via controlling their separation distance *d*. Our experimental and simulation results reveal that the PL intensity of the Au NB can be increased by the localized field enhancement from the plasmonic resonance of a Ag NW when *d* is reduced from 15 to 7 nm (we did not observe enhancements of the PL for d > 15 nm). When the separation distance *d* is smaller than 7 nm, the gap plasmons due to the dipole−dipole interaction between the Ag NW and the Au NB dominate, resulting in a new PL peak around the resonance wavelength of the gap plasmon modes and quenching of the PL. Although this work demonstrates only the enhancement and the modulation of PL of Au NBs by Ag NWs, a similar

DOI: 10.1021/acsphotonics.5b00341
ACS Photonics 2015, 2, 1348−1354

phenomenon can be expected when utilizing other plasmonic materials to enhance the PL of metallic structures. The tunable gap plasmon modes may also be used for experiments involving optical absorbers,[34] enhanced fluorescence emissions,[35] and others. Moreover, the gap plasmons may modulate the emission direction of the PL,[16,18,35] and therefore we plan to investigate the angular distribution of the gap plasmon modulated PL emission in the near future.

METHODS

Synthesis of Au Microplates. The Au microplates were prepared by following a procedure reported in the literature.[26] We first heated 5 mL of ethylene glycol (EG, purchased from J.T. Baker) in a glass vial for 1 h and then added 0.83 mL of $HAuCl_4$ (Sigma-Aldrich) solution in EG (0.2 M) and 2.5 mL of PVP (MW = 55 000, Aldrich) solution in EG (222 mg/mL). The solution was continuously stirred for 1 h at 160 °C to form a mixture of Au microplates and nanoparticles. To separate the microplates from the nanoparticles, 10 mL of PVP solution in ethanol (0.25 g/mL) and 30 mL of PVP aqueous solution (0.25 g/mL) were added in the solution containing the microplates and the nanoparticles. After 6 h, the microplates settled around the bottom of the glass vial, while the nanoparticles were left in the top ethanol phase of the solution. We discarded the supernatant and redispersed the microplates in PVP aqueous solution (0.25 g/mL).

Fabrication of Au NBs by Nanoskiving. We followed a procedure reported in the literature to fabricate Au NBs,[27] as shown in Figure 1. A flat piece of epoxy (Epo-fix, Electron Microscopy Sciences) was prepared by puddle-casting the mixture of epoxy prepolymer and its hardener on a Si wafer. After curing the polymer at room temperature for 12 h, we separated the epoxy slab from the wafer and drop-casted the suspensions of Au microplates on the flat slide of the slab. After drying, the slab with the microplates was rinsed with ethanol and ultrapure water (18 MΩ·cm) carefully to clean the PVP and EG residues, without removing the microplates from the slab. After drying again, we used a razor blade to cut the slab with the microplates into small strips. We embedded the strips with the mixture of epoxy prepolymer and its hardener in a polyethylene mode to form an epoxy block. After curing, we trimmed the epoxy block to fit the size of the diamond knife (Diatome Ultra 35) and sectioned the block using the ultramicrotome to generate 50 nm thick films containing the Au NBs.

Deposition of Al_2O_3 by ALD. The Al_2O_3 was deposited on the SiO_2/Si substrate with Au NBs by utilizing a Savannah 100 and 200 system (Cambridge Nano Tech Inc.) at 90 °C using trimethylaluminum [$Al(CH_3)_3$] and water as precursors and N_2 as the carrier gas with a flow rate of 20 SCCM (cubic centimeter per minute). During the deposition, the pressure in the reaction chamber was maintained at 0.35 mbar. Each deposition cycle contained a pulse of $Al(CH_3)_3$ for 15 ms and a subsequent purging of N_2 for 1 min, followed by a pulse of water for 15 ms and a subsequent purging of N_2 for 30 s. The growth rate of each cycle was about 0.11 nm. The thickness of Al_2O_3 was controlled by the total numbers of the deposition cycles.

Synthesis of Ag NWs. We synthesized Ag NWs by following a procedure reported by Xia's group.[25] We first heated 5 mL of EG under magnetic starring at 150 °C for 1 h and then added 40 μL of the solution of $CuCl_2$ (>99.999%, Aldrich) dissolved in EG (4 mM). After stirring for 15 min, 1.5 mL of PVP solution in EG (147 mM) and 1.5 mL of $AgNO_3$ (>99%, Sigma-Aldrich) solution in EG (94 mM) were added into the solution simultaneously. After 1 h of stirring, the reaction was quenched by cooling the reaction vial in a water bath at room temperature. The resulting Ag NWs were washed with ultrapure water and ethanol to remove PVP and EG residues and were stored in ethanol after cleaning.

PL Measurements. The PL spectra and images of the samples were acquired using a CRM200 confocal Raman microscope (WITec), in which the spectra were dispersed by a 150 lines/mm grating and collected using a TE-cooled CCD (Andor DV 401-BV-351). The microscope contains a high-resolution spectrograph (0.55 nm/pixel), which gives an accuracy of the peak positions in the spectrum of within ±1 nm. During the PL measurement, a linearly polarized laser with a wavelength of 457 nm and power of 50 μW was focused on the surface of the sample through a Zeiss Epiplan objective (100×, NA = 0.75). All PL spectra were obtained with an integration time of 5 s after focusing the laser at the given region of interest. The PL images were acquired by integrating the complete PL spectra for an area of 6 × 6 μm^2 with 150 × 150 pixels per image.

Theoretical Simulations. We used a classic transfer matrix method (TMM) to calculate the transmission shown in Figure 6a. During the calculation, the Ag NW and Au NB were simplified as a 70 nm Ag film and a 50 nm Au film, respectively. The 300 nm oxide layer on the Si substrate was also considered. Thus, the transmittance is calculated through the air−Ag-Al_2O_3−Au-SiO_2−Si substrate structure with a variation of the Al_2O_3 film thickness and with $k = k_0\lambda/D$ (D = 70 nm). To simulate the scattering spectra (Figure 6b) and the field distribution (Figures 6c−f), three-dimensional finite-difference time-domain (3D-FDTD) simulations were performed using Lumerical FDTD solution v8.5. Perfectly matched layers were defined as boundary conditions of our simulation volume at a distance with respect to the structure of at least one wavelength. In the simulation, a fine mesh size of 0.5 nm × 0.5 nm × 0.25 nm was used for the combined nanostructure. A total-field scattered-field (TFSF) source with a beam size of 350 nm × 350 nm illuminated the structure, and the scattering spectra were recorded 200 nm above the source. During the FDTD simulation, the Ag NW edges were set to be 72 nm and the Ag NW was rounded at the corners with a radius of 10 nm (estimated from the SEM images). The Au NB was 50 nm in height and 150 nm in width. A oxide layer of SiO_2 on the Si substrate (300 nm) was also included. For both TMM calculation and FDTD simulation, the dielectrics of Ag and Au were from ref 36, and the dielectrics of Al_2O_3, SiO_2, and Si were from ref 37.

ASSOCIATED CONTENT

Supporting Information

The Supporting Information is available free of charge on the ACS Publications website at DOI: 10.1021/acsphotonics.5b00341.

(S1) E_z field distributions for both peak I and peak II. (S2) Determination of the absolute PL emission rate. (S3) The diameter effect of PL spectra from the Au NB−Ag NW cross-like structures. (S4) FDTD-simulated field distributions at 457 and 520 nm with different gap d (PDF)

DOI: 10.1021/acsphotonics.5b00341
ACS Photonics 2015, 2, 1348−1354

AUTHOR INFORMATION

Corresponding Author

*E-mail: chmnca@nus.edu.sg.

Author Contributions

#A. Wan and T. Wang contributed equally to this work.

Notes

The authors declare no competing financial interest.

ACKNOWLEDGMENTS

We acknowledge the National Research Foundation (NRF) for supporting this research under the Competitive Research Programme (CRP) program (award NRF-CRP 8-2011-07).

REFERENCES

(1) Wang, H.; Huff, T. B.; Zweifel, D. A.; He, W.; Low, P. S.; Wei, A.; Cheng, J.-X. In vitro and In vivo two-photon luminescence imaging of single gold nanorods. *Proc. Natl. Acad. Sci. U. S. A.* **2005**, *102*, 15752−15756.

(2) He, H.; Xie, C.; Ren, J. Nonbleaching fluorescence of gold nanoparticles and its applications in cancer cell imaging. *Anal. Chem.* **2008**, *80*, 5951−5957.

(3) Wu, X.; Ming, T.; Wang, X.; Wang, P.; Wang, J.; Chen, J. High-photoluminescence-yield gold nanocubes: For cell imaging and photothermal therapy. *ACS Nano* **2010**, *4*, 113−120.

(4) Tong, L.; Cobley, C. M.; Chen, J.; Xia, Y.; Cheng, J.-X. Bright three-photon luminescence from gold/silver alloyed nanostructures for bioimaging with negligible photothermal toxicity. *Angew. Chem., Int. Ed.* **2010**, *49*, 3485−3488.

(5) Lu, G.; Hou, L.; Zhang, T.; Liu, J.; Shen, H.; Luo, C.; Gong, Q. Plasmonic sensing via photoluminescence of individual gold nanorod. *J. Phys. Chem. C* **2012**, *116*, 25509−25516.

(6) Chan, P.-H.; Ghosh, B.; Lai, H.-Z.; Peng, H.-L.; Mong, K. K. T.; Chen, Y.-C. Photoluminescent gold nanoclusters as sensing probes for uropathogenic escherichia coli. *PLoS One* **2013**, *8*, e58064.

(7) Mühlschlegel, P.; Eisler, H. J.; Martin, O. J. F.; Hecht, B.; Pohl, D. W. Resonant optical antennas. *Science* **2005**, *308*, 1607−1609.

(8) Imura, K.; Nagahara, T.; Okamoto, H. Near-field two-photon-induced photoluminescence from single gold nanorods and imaging of plasmon modes. *J. Phys. Chem. B* **2005**, *109*, 13214−13220.

(9) Ghenuche, P.; Cherukulappurath, S.; Taminiau, T. H.; van Hulst, N. F.; Quidant, R. Spectroscopic mode mapping of resonant plasmon nanoantennas. *Phys. Rev. Lett.* **2008**, *101*, 116805.

(10) Mooradian, A. Photoluminescence of metals. *Phys. Rev. Lett.* **1969**, *22*, 185−187.

(11) Beversluis, M. R.; Bouhelier, A.; Novotny, L. Continuum generation from single gold nanostructures through near-Field mediated intraband transitions. *Phys. Rev. B: Condens. Matter Mater. Phys.* **2003**, *68*, 115433.

(12) Dulkeith, E.; Niedereichholz, T.; Klar, T. A.; Feldmann, J.; von Plessen, G.; Gittins, D. I.; Mayya, K. S.; Caruso, F. Plasmon emission in photoexcited gold nanoparticles. *Phys. Rev. B: Condens. Matter Mater. Phys.* **2004**, *70*, 205424.

(13) Yorulmaz, M.; Khatua, S.; Zijlstra, P.; Gaiduk, A.; Orrit, M. Luminescence quantum yield of single gold nanorods. *Nano Lett.* **2012**, *12*, 4385−4391.

(14) Fang, Y.; Chang, W.-S.; Willingham, B.; Swanglap, P.; Dominguez-Medina, S.; Link, S. Plasmon emission quantum yield of single gold nanorods as a function of aspect ratio. *ACS Nano* **2012**, *6*, 7177−7184.

(15) Bouhelier, A.; Bachelot, R.; Lerondel, G.; Kostcheev, S.; Royer, P.; Wiederrecht, G. P. Surface Plasmon Characteristics of Tunable Photoluminescence in Single Gold Nanorods. *Phys. Rev. Lett.* **2005**, *95*, 267405.

(16) Hu, H.; Duan, H.; Yang, J. K. W.; Shen, Z. X. Plasmon-modulated photoluminescence of individual gold nanostructures. *ACS Nano* **2012**, *6*, 10147−10155.

(17) Gao, N.; Chen, Y.; Li, L.; Guan, Z.; Zhao, T.; Zhou, N.; Yuan, P.; Yao, S. Q.; Xu, Q.-H. Shape-dependent two-photon photoluminescence of single gold nanoparticles. *J. Phys. Chem. C* **2014**, *118*, 13904−13911.

(18) Hu, H.; Akimov, Y. A.; Duan, H.; Li, X.; Liao, M.; Tan, R. L. S.; Wu, L.; Chen, H.; Fan, H.; Bai, P.; Lee, P. S.; Yang, J. K. W.; Shen, Z. X. Photoluminescence via gap plasmons between single silver nanowires and a thin gold film. *Nanoscale* **2013**, *5*, 12086−12091.

(19) Lumdee, C.; Yun, B.; Kik, P. G. Gap-plasmon enhanced gold nanoparticle photoluminescence. *ACS Photonics* **2014**, *1*, 1224−1230.

(20) Andersen, S. K. H.; Pors, A.; Bozhevolnyi, S. I. Gold photoluminescence wavelength and polarization engineering. *ACS Photonics* **2015**, *2*, 432−438.

(21) Anger, P.; Bharadwaj, P.; Novotny, L. Enhancement and Quenching of Single-Molecule Fluorescence. *Phys. Rev. Lett.* **2006**, *96*, 113002.

(22) Zhao, L.; Ming, T.; Chen, H.; Liang, Y.; Wang, J. Plasmon-induced modulation of the emission spectra of the fluorescence molecules near gold nanorods. *Nanoscale* **2011**, *3*, 3849−3859.

(23) Ringler, M.; Schwemer, A.; Wunderlich, M.; Nichtl, A.; Kürzinger, K.; Klar, T. A.; Feldmann, J. Shaping emission spectra of fluorescence molecules with single plasmonic nanoresonators. *Phys. Rev. Lett.* **2008**, *100*, 203002.

(24) Bourret, G. R.; Ozel, T.; Blaber, M.; Shade, C. M.; Schatz, G. C.; Mirkin, C. A. long-range plasmophore rulers. *Nano Lett.* **2013**, *13*, 2270−2275.

(25) Korte, K. E.; Skrabalak, S. E.; Xia, Y. Rapid synthesis of silver nanowires through a CuCl- or $CuCl_2$-mediated polyol process. *J. Mater. Chem.* **2008**, *18*, 437−441.

(26) Kan, C.; Zhu, X.; Wang, G. Single-crystalline gold microplates: synthesis, characterization, and thermal stability. *J. Phys. Chem. B* **2006**, *110*, 4651−4656.

(27) Wiley, B. J.; Lipomi, D. J.; Bao, J. M.; Capasso, F.; Whitesides, G. M. Fabrication of surface plasmon resonators by nanoskiving single-crystalline gold microplates. *Nano Lett.* **2008**, *8*, 3023−3028.

(28) Noguez, C. Surface Plasmons on Metal Nanoparticles: The influence of shape and physical environment. *J. Phys. Chem. C* **2007**, *111*, 3806−3819.

(29) Mock, J. J.; Hill, R. T.; Degiron, A.; Zauscher, S.; Chilkoti, A.; Smith, D. R. Distance-dependant plasmon resonant coupling between a gold nanoparticle and gold film. *Nano Lett.* **2008**, *8*, 2245−2252.

(30) Hu, M.; Ghoshal, A.; Marquez, M.; Kik, P. G. Single particle spectroscopy study of metal-film-induced tuning of silver nanoparticle plasmon resonances. *J. Phys. Chem. C* **2010**, *114*, 7509−7514.

(31) Lassiter, J. B.; McGuire, F.; Mock, J. J.; Ciracì, C.; Hill, R. T.; Wiley, B. J.; Chilkoti, A.; Smith, D. R. Plasmonic waveguide modes of film-coupled metallic nanocubes. *Nano Lett.* **2013**, *13*, 5866−5872.

(32) Lipomi, D. J.; Ilievski, F.; Wiley, B. J.; Deotare, P. B.; Lončar, M.; Whitesides, G. M. Integrated fabrication and magnetic positioning of metallic and polymeric nanowires embedded in thin epoxy slabs. *ACS Nano* **2009**, *3*, 3315−3325.

(33) Dickey, M. D.; Lipomi, D. J.; Bracher, P. J.; Whitesides, G. M. Fabrication of electrically addressable nanowires with 30-nm spacing using micromolding and nanoskiving. *Nano Lett.* **2008**, *8*, 4568−4573.

(34) Hao, J.; Wang, J.; Liu, X.; Padilla, W. J.; Zhou, L.; Qiu, M. High Performance Optical Absorber Based on a Plasmonic Metamaterials. *Appl. Phys. Lett.* **2010**, *96*, 251104.

(35) Akselrod, G. M.; Argyropoulos, C.; Hoang, T. B.; Ciracì, C.; Fang, C.; Huang, J.; Smith, D. R.; Mikkelsen, M. H. Probing the mechanisms of large Purcell enhancement in plasmonic nanoantennas. *Nat. Photonics* **2014**, *8*, 835−840.

(36) Johnson, P. B.; Christy, R. W. Optical Constants of the Noble Metals. *Phys. Rev. B* **1972**, *6*, 4370.

(37) Palik, E. D. *Handbook of Optical Constants of Solids*; Academic Press: San Diego, CA, 1998.

DOI: 10.1021/acsphotonics.5b00341
ACS Photonics 2015, 2, 1348−1354